Journal of Power Sources 248 (2014) 565–569

Contents lists available at ScienceDirect

Journal of Power Sources

journal homepage: www.elsevier.com/locate/jpowsour

Short communication

Synthesis of carbon microspheres loaded with manganese oxide as air cathode in alkaline media

Hailing Gao [a], Zhenya Li [b], Xue Qin [a,*]

[a] School of Science, Tianjin University, Tianjin 300072, China
[b] School of Chemical Engineering and Technology, Tianjin University, Tianjin 300072, China

HIGHLIGHTS

- Carbon microspheres have been prepared by reflux-calcinations.
- A kind of catalyst MnO_x loaded on the carbon microspheres has been studied.
- The composite catalyst's BET surface is1278 $m^2\ g^{-1}$.
- The apparent exchange current density of the composite catalyst electrode is 0.649 mA cm^{-2}.
- The mechanism of oxygen reduction is a 2e pathway.

ARTICLE INFO

Article history:
Received 21 May 2013
Received in revised form
29 July 2013
Accepted 7 September 2013
Available online 27 September 2013

Keywords:
Carbon microspheres
Manganese dioxide
Oxygen reduction reaction
Air cathode
Alkaline

ABSTRACT

Carbon microspheres with large surface have been synthesized from sucrose in H_2SO_4 solution by reflux-calcinations method. The catalyst of the manganese oxide loaded on carbon microspheres surface demonstrates significant catalytic activity for the oxygen reduction reaction in alkaline media and the mechanism of oxygen reduction is a 2e pathway. It shows an enhanced efficiency for electrochemical properties on active surface and apparent exchange current density 0.649 mA cm^{-2} (comes from the Tafel plots) for oxygen reduction reaction. This enhancement results from the large reaction area of the 7.32 wt.% manganese oxide loaded on carbon microspheres as well as the porous structures between this composite, which can significantly promote the efficient diffusion.

© 2013 Elsevier B.V. All rights reserved.

1. Introduction

With ever-increasing widespread applications of the metal-air and fuel cells in alkaline, the catalyst material for oxygen reduction reaction (ORR) on air cathode is increasingly urgent. General requirements of the catalyst material on air cathode are good catalytic activity for ORR, electrolyte corrosion resistance, great conductivity and large specific surface area. During past decades, a variety of non-precious metals [1] or non-platinum catalysts [2,3] have been studied, while manganese oxides [4–9] have been identified as the most promising candidates for the ORR catalyst because of their low cost, abundance and the considerable catalytic activity toward electrochemical ORR. Early reports have shown that the catalytic performance of MnO_x follows the sequence of $Mn_5O_8 < Mn_3O_4 < Mn_2O_3 < MnOOH$ and that among MnO_2 phases, the performance sequence turns to β- < λ- < γ- < α-MnO_2 [10,11]. Four commercial MnO_2 powders (Tronox, Sigma–Aldrich, Merck and Riedel de Haen) have been published by Gyenge and Drillet [12], whose electrochemical ORR performance are similar to our catalysts reported in the following, but our catalysts show much bigger reduction current for ORR and higher electrochemically active reaction area compared to the four commercial MnO_2 powders. The studies of manganese oxides applied in metal-air and fuel cells suggest that the crystal's structure, particle size, synthesis method and the support material can significantly affect the catalytic activity for ORR.

In addition to catalyst preparation, the choice of a suitable catalyst support plays a key role for ORR on air cathode. Carbon-related materials can enhance the catalytic activity and reduce the use of noble metal catalysts. For example, carbon nanotube [13],

* Corresponding author. Tel.: +86 022 27403670.
E-mail address: qinxue@tju.edu.cn (X. Qin).

0378-7753/$ – see front matter © 2013 Elsevier B.V. All rights reserved.
http://dx.doi.org/10.1016/j.jpowsour.2013.09.033

graphene [14], fullerenes [15], nitrogen-doped carbon spheres [16], carbon [17], carbon spheres [18] have been researched. We prepared a kind of support, carbon microspheres (CMs), with the BET area 1110 $m^2\ g^{-1}$ have been used for the support of manganese oxide in this paper.

In this paper, the CMs are synthesized by reflux-calcinations method. The as-prepared CMs are used as manganese oxide catalyst's support for ORR in alkaline media. The composites have excellent electrochemical properties for ORR according to the electrochemical measurements steady-state polarization, cyclic voltammograms and impedance spectra.

2. Experimental

Synthesis of CMs: (1) 5 wt.% sucrose in 6 mol L^{-1} H_2SO_4 solution was stirred and heated to reflux for 24 h, then the mixture was filtered and washed with deionized water, followed by dried to obtain the precursor of CMs; (2) the precursor was calcined at 1000 °C for 2 h in muffle furnace and cooled to room temperature in nitrogen; (3) the above samples were activated at 450 °C for 2 h in air.

Manganese oxide loaded on CMs was made by dissolving commercial 50 wt.% $Mn(NO_3)_2$ solution in an aqueous suspension of CMs powder used after ultrasonically blending. Then, the solvent was evaporated and the composite powder was submitted to thermal decomposition under nitrogen at 320 °C [19] for 40 min. The catalyst with 3.13 wt.% manganese oxide was obtained by reacting 0.022 g $Mn(NO_3)_2$ with 0.1 g CMs (denoted as: 3.13%MnO_x/CMs, from the test of TGA). The catalysts with different mass fraction of manganese oxide 7.32%MnO_x/CMs and 13.04%MnO_x/CMs were prepared by changing the weight ratio of $Mn(NO_3)_2$ to CMs. (The mass fraction of raw material $Mn(NO_3)_2$ are 10%, 20%, 40% respectively to 3.13%MnO_x/CMs, 7.32%MnO_x/CMs and 13.04%MnO_x/CMs.)

The working electrode (WE1) for the electrochemical measurements of polarization curves and impedance spectroscopy was consisted from a catalyst layer, a gas diffusion layer and a current accumulating matrix, which was prepared as following: catalyst, acetylene black and PTFE in the 8:1:1 mass ratio in ethanol to form a homogeneous paste that was rolled into a 0.3 mm thick sheet. The gas diffusion layer was prepared as described in document [11]. The working electrode was finished by pressing the catalyst layer and gas diffusion layer onto a nickel mesh at 200 kg cm^{-2} [20].

The other working electrode (WE2) for cyclic voltammograms (CVs) measurement was fabricated by casting the ethanol impregnated as-prepared MnO_x/CMs catalysts ink onto a glass carbon (GC) electrode (3 mm diameter), which was then allowed to dry under an infrared lamp.

Electrochemical measurements were performed in a three-electrode cell [21] with WE1 (one side to the air, one side to the electrolyte) or WE2 (CVs) as working electrode, a Ni-mesh served as counter electrode and Hg/HgO electrode used as reference electrode in 6 M KOH solution.

3. Results and discussion

All samples' steady-state polarization curves can be seen from Fig. 1a, in which the effect of manganese oxide on the CMs is quite obvious. The electrode with 7.32%MnO_x/CMs owns lowest overpotential and highest reduction current for ORR compared to others, demonstrating the best performance for ORR. In order to further verify this result, the Tafel plots of all samples are emerged in Fig. 1b. The apparent exchange current density from Tafel plots are 0.048 mA cm^{-2} for CMs, 0.25 mA cm^{-2} for 3.13%MnO_x/CMs, 0.649 mA cm^{-2} for 7.32%MnO_x/CMs and 0.631 mA cm^{-2} for 13.04%

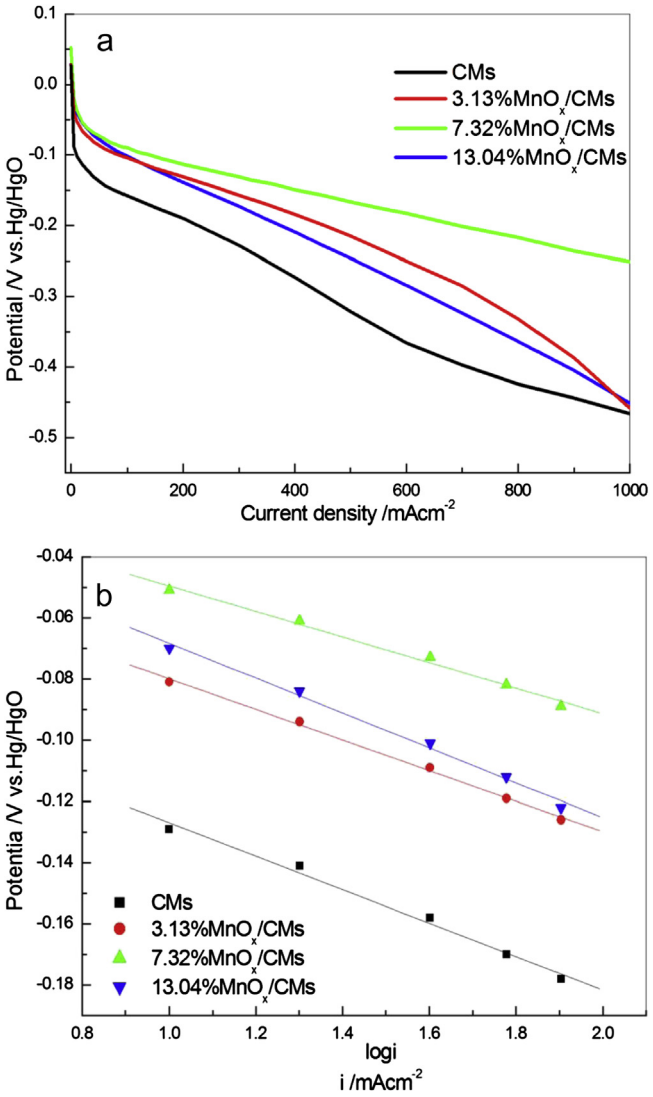

Fig. 1. Steady-state polarization curves for the four air cathodes in air saturated in 6 M KOH (a) and Tafel plots of the four samples (b). 298 K.

MnO_x/CMs, respectively. The number value of 13.04%MnO_x/CMs is similar to 7.32%MnO_x/CMs, but the performance tests show that 7.32%MnO_x/CMs is better than 13.04%MnO_x/CMs from the following tests. It can be explained that the larger loading leads to lower electrical conductivity and bigger ohmic polarization than 7.32%MnO_x/CMs. What's more, at the large current density especially after 200 mA cm^{-2}, 13.04%MnO_x/CMs shows more obvious ohmic potential drop, so from the overall terms, the performance shows that 7.32% is better than 13.04%. The result suggests that the 7.32%MnO_x/CMs air cathode performs a highest catalytic activity, which is suitable for cathode materials.

To confirm the compound of this best catalyst, the XRD patterns of the CMs (a) and 7.32%MnO_x/CMs (b) are shown in Fig. 2. Fig. 2a shows the standard pattern of carbon with the presence of two peaks at $2\theta = 26°$ and 44°, which are reflections from the (002) and (101) planes (JCPDS No. 75-1621). The peaks at 2θ = 28.7°, 38.8°, 45°, 59° and 60° are indexed to the (110), (101), (210), (211) and (220) facets of MnO_2 (JCPDS PDF 01-0799) as shown in Fig. 2b. Some peaks of MnO_2 are not obvious because these are covered by carbon's wide peak. Other peaks at 2θ = 32.3°, 36.1° can be attributed to the Mn_3O_4 (JCPDS PDF 24-0734). Obviously the amount of Mn_3O_4 in the catalyst is very low. These results suggest

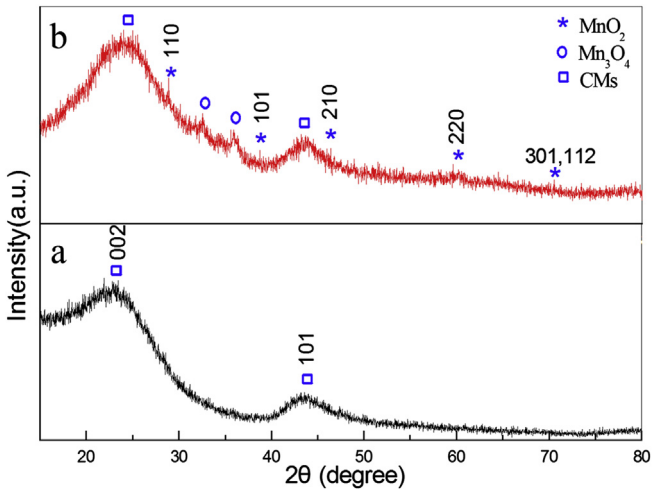

Fig. 2. XRD patterns of CMs (a) and 7.32%MnO_x/CMs (b).

that manganese oxides are successfully deposited on the CMs and the manganese oxides are mainly MnO_2.

Fig. 3 shows RHTEM images of the as-synthesized CMs (a, b) and 7.32%MnO_x/CMs (c, d) catalyst. It can be observed from Fig. 3a that the CMs with diameter about 400 nm have smooth edge (Fig. 3b). Fig. 3c shows the image of 7.32%MnO_x/CMs, whose diameter are relatively larger than CMs, due to the homogeneous distribution on the surface of CMs by manganese oxides. The rough surface of 7.32% MnO_x/CMs (Fig. 3d) stems from the manganese oxides' attachment, compared with CMs' smooth edge.

The N_2 adsorption/desorption isotherm of 7.32%MnO_x/CMs studies reveals a typical type IV classification which is characteristic of micropore materials as shown in Fig. 4a. The pore-size distribution is centered at 0–2 nm while relatively lower proportion peaks are centered at 6 and 15 nm, as observed in Fig. 4b. The nano-sized pores in the mesoporous structure significantly allow efficient diffusion which enhances the electrode/electrolyte contact area [22]. The BET surface area of the sample is observed to be 1278 $m^2\ g^{-1}$ which is higher than that of CMs (1110 $m^2\ g^{-1}$). These characteristics not only increase the reaction area of the ORR but also improve the electrochemical activity.

Fig. 5 shows the CVs with the potential range from −0.65 to 0.2 V of 7.32%MnO_x/CMs electrode in different ambience in 6 M KOH: in N_2-purged (a), in air saturated (line A) and in 0.5 mM H_2O_2 of 6 M KOH (line B) (b), at different scan rates (c). The CVs exhibit two cathodic and anodic peaks, labeled as p_c and p_a, respectively (especially pronounced at 1 mV s^{-1} in Fig. 5c). The p_c and p_a peak potentials are consistent for all different ambience: around −0.4 V (for p_c) and about −0.2 V (for p_a), respectively. From the literature [12], it can be inferred that the presence of a voltammetric reduction peak at −0.4 V vs. Hg/HgO is a typical feature of electroactive MnO_2 sample and the oxidation p_a peak at −0.2 V is attributed to the forming MnOOH. The objective of Fig. 5a is to investigate the

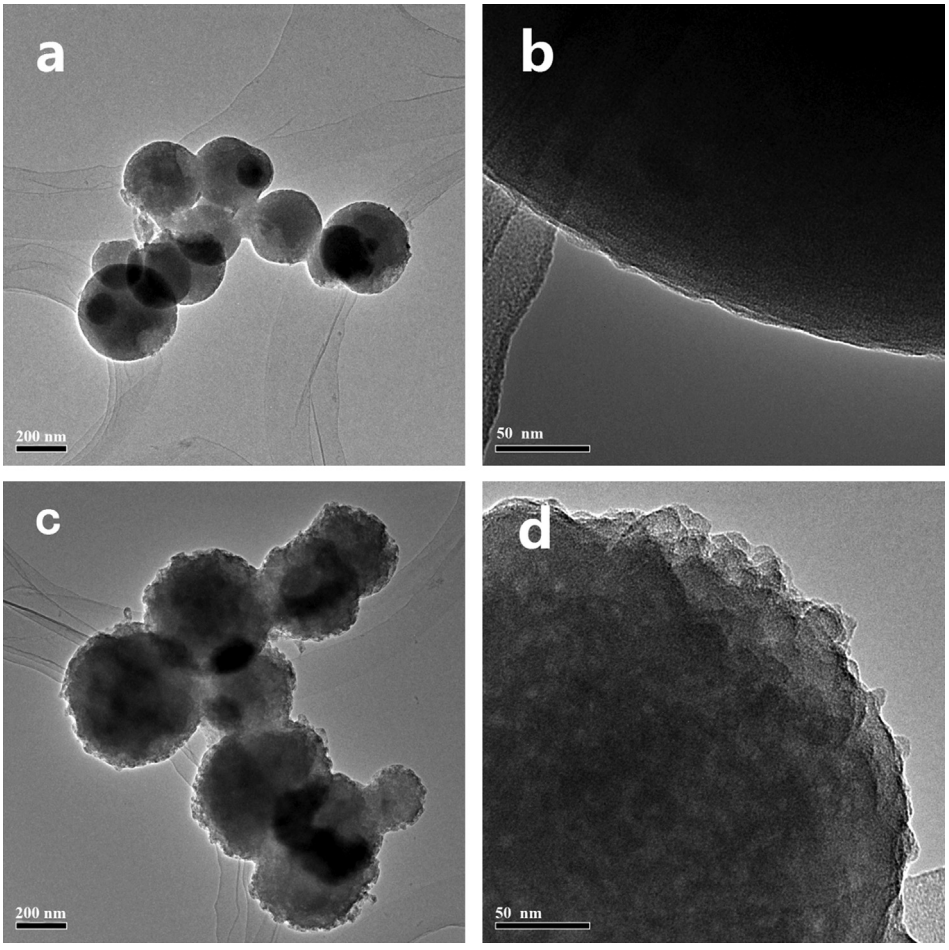

Fig. 3. RHTEM images of CMs (a, b) and 7.32%MnO_x/CMs (c, d).

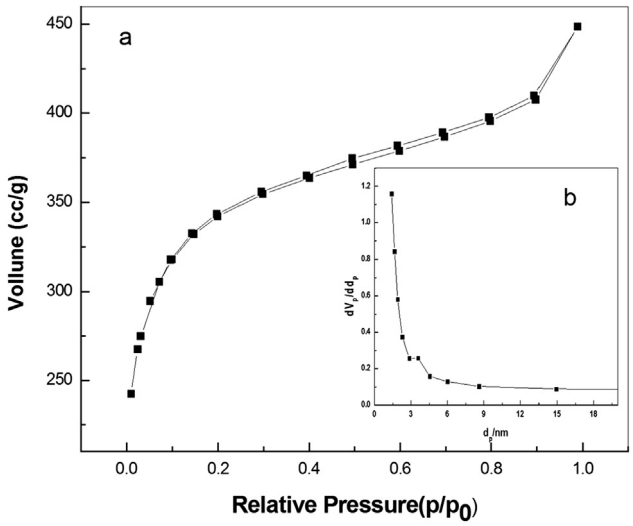

Fig. 4. Nitrogen adsorption isotherm (a) and pore size distribution (b) of the 7.32% MnO_x/CMs.

intrinsic electrochemical behavior of the MnO_2 powders in the absence of oxygen. p1 and the characteristic peak of H_2O_2 appear at the same potential −0.2 V, but the peak current of H_2O_2 is much higher than p1 as shown in Fig. 5b. It has been reported that manganese oxides are highly catalytically active toward the peroxide decomposition. [11,23–26] Hence there is a presence of the intermediate H_2O_2 formed on MnO_2 at the first step, and it can be consumed almost instantaneously.

Based on Fig. 5, the ORR mechanism on manganese oxides can be identified by a 2-electron reduction, the peak around −0.2 V could attributed to the reduction of O_2 to HO_2^- as described in Eq. (1) and the peak around −0.4 V shows the electrochemically transition of HO_2^- to OH^- (Eq. (2)) [26,27].

$$O_2 + H_2O + 2e^- \rightarrow HO_2^- + OH^- \quad (1)$$

$$HO_2^- + H_2O + 2e^- \rightarrow 3OH^- \quad (2)$$

It is common in the literature to attribute two successive cathodic peaks (p_c and p2 in Fig. 5c at 1 mV s^{-1}) to the sequential reduction of Mn^{4+} and Mn^{3+} species according to the mechanism as the following equations [11,12,27]:

$$MnO_2 + H_2O + e^- \Leftrightarrow MnOOH + OH^- \quad (3)$$

$$MnOOH + O_2 \Leftrightarrow MnOOH\cdots O_2 \quad (4)$$

$$MnOOH\cdots O_2 + e^- \Leftrightarrow MnO_2 + HO_2^- \quad (5)$$

The total reaction of Eqs. (3)–(5) equals to Eq. (1) with an overall 2e transfer. For reaction (1), O_2 is reduced to HO_2^- which is catalyzed by the largely unreduced MnO_2 surface and by the CMs support [12].

The p1 and its associated p2 peaks could be explained that they are due to the second electron transfer step generating Mn^{2+} species from MnOOH (Eq. (3)) [12]. The other explanation is due to the CMs support effect, which can play a role as well in the magnitude of the p1 and p2 peaks observed in the present study [12]. With increasing scan rate, p1 and p2 are gradually become unobvious.

Additionally, the reduction peaks shift slightly to more negative potentials at higher scan rates as illustrated in Fig. 5c, demonstrating this composite catalyst has excellent reproducibility.

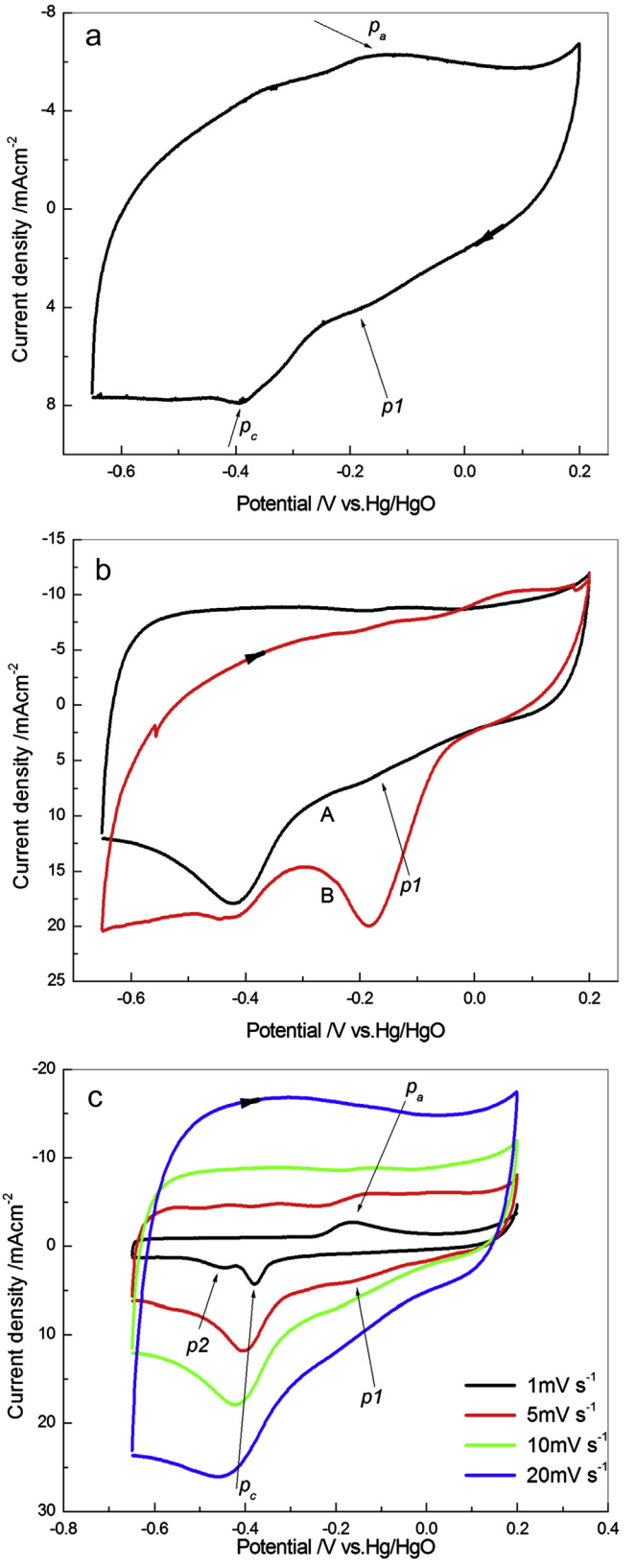

Fig. 5. CVs of the 7.32%MnO_x/CMs air cathode in different ambience in 6 M KOH: in N_2-purged at scan rate 10 mV s^{-1} (a), in air saturated (line A) and in 0.5 mM H_2O_2 of 6 M KOH (line B) at scan rate 10 mV s^{-1} (b), at different scan rates (c) (GC electrode as the working electrode, Hg/HgO as the reference electrode, a sintered Ni-mesh as counter electrode). 298 K.

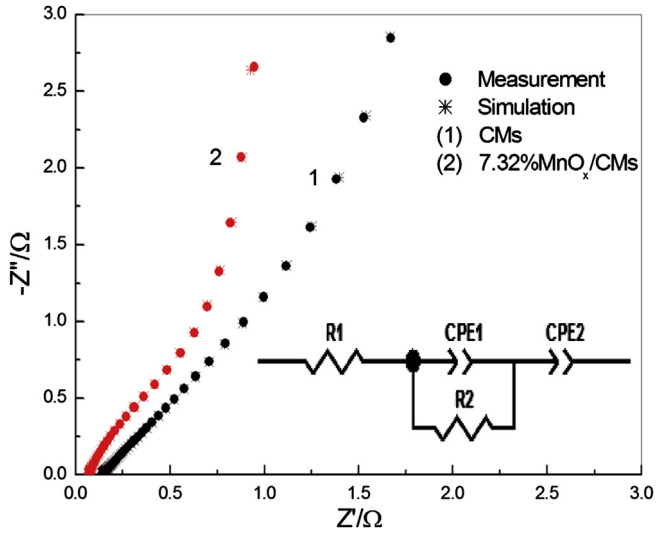

Fig. 6. Impedance spectra of the CMs and 7.32%MnO_x/CMs in 6 M KOH and the equivalent circuit of the electrodes (inset). 298 K.

Furthermore, the cathodic peak current increase with the scan rates and are proportional to the square roots of scan rates from 1 to 20 mV s^{-1}, which indicates a diffusion controlled for the ORR at electrode with 7.32%MnO_x/CMs.

In Fig. 6, the impedance spectra of the CMs and 7.32%MnO_x/CMs electrodes are consisted of one semicircle and a slope. Inset is the equivalent circuit of the electrodes, where R1, R2, CPE1 and CPE2 are denoted as solution resistance, electrochemical reaction resistance, double layer capacitance and the diffusion capacitance, respectively. Due to the porous morphology of electrodes, a constant phase element (CPE) replaces the capacitor elements reasonably. A CPE is usually defined as $\{Y(jw)\}^{-1}$. A nonlinear, least-square fitting calculation is performed using the equivalent circuit. For CMs electrode, the R2 and CPE1 value (T) are 10.15 Ω cm^2 and 0.386 F cm^{-2}, and 7.32%MnO_x/CMs electrode are 1.02 Ω cm^2 and 0.426 F cm^{-2}. The R2 of the 7.32%MnO_x/CMs electrode is obviously much lower than that of the CMs electrode. Therefore, it is concluded that 7.32%MnO_x/CMs has higher electrochemical activity for ORR, which is consistent with the polarization curves and CVs. In addition, the CPE1 value (T) is the value of the double layer capacitance of the electrode, which relates to the true electrochemical reaction areas of the electrode. The double layer capacitance of 7.32%MnO_x/CMs electrode is larger than that of the CMs electrode obviously which means 7.32%MnO_x/CMs electrodes has larger reaction area.

4. Conclusions

A facile method for the synthesis of CMs has been studied by reflux-calcination. The manganese oxide loaded on CMs catalyst is prepared by impregnating and manganese oxide appears homogeneously immobilized on CMs surface. The 7.32%MnO_x/CMs composite catalyst exhibits a much higher catalytic activity on large surface and apparent exchange current density for ORR in alkaline media, and the oxygen reduction on manganese oxides undergoes a two-electron (2e) pathway, which has potential applications in metal-air and fuel cells.

Acknowledgments

The authors gratefully acknowledge the financial support from the National Natural Science Foundation of China (20603024) and the Open Project of Key Lab Adv. Energy Mat. Chem. (Nankai Univ.) (KLAEMC-OP201201).

References

[1] V. Neburchilov, H.J. Wang, J.J. Martin, Wei. Qu, J. Power Sources 195 (2010) 1271–1291.
[2] H. Meng, P.K. Shen, Electrochem. Commun. 8 (2006) 588–594.
[3] J.W. Fergus, J. Power Sources 195 (2010) 939–954.
[4] C.N. Chervin, J.W. Long, N.L. Brandell, J.M. Wallace1, N.W. Kucko, D.R. Rolison, J. Power Sources 207 (2012) 191–198.
[5] N. Omindea, N. Bartlett, X.Q. Yang, D.Y. Qu, J. Power Sources 185 (2008) 747–753.
[6] J.X. Li, N. Wang, Y. Zhao, Y.H. Ding, L.H. Guan, Electrochem. Commun. 13 (2011) 698–700.
[7] J.M. Kim, Y.S. Huh, Y.-K. Han, M.S. Cho, H.J. Kim, Electrochem. Commun. 14 (2012) 32–35.
[8] W. Sun, A. Hsu, R.R. Chen, J. Power Sources 196 (2011) 627–635.
[9] R.X. Feng, H. Dong, Y.D. Wang, X.P. Ai, Y.L. Cao, H.X. Yang, Electrochem. Commun. 7 (2005) 449–452.
[10] (a) F.H.B. Lima, M.L. Calegaro, E.A. Ticianelli, J. Electroanal. Chem. 590 (2006) 152–160;
(b) F.H.B. Lima, M.L. Calegaro, E.A. Ticianelli, Electrochim. Acta 52 (2007) 3732–3738.
[11] Y.L. Cao, H.X. Yang, X.P. Ai, L.F. Xiao, J. Electroanal. Chem. 557 (2003) 127–134.
[12] E.L. Gyenge, J.F. Drillet, J. Electrochem Soc. 159 (2012) F23–F34.
[13] M. Liu, S. Kharkwal, H.Y. Ng, S.F.Y. Li, Biosens. Bioelectron. 26 (2011) 4728–4732.
[14] Q. Wen, S.Y. Wang, J. Yan, L.J. Cong, Z.C. Pan, Y.M. Ren, Z.J. Fan, J. Power Sources 216 (2012) 187–191.
[15] H.W. Kroto, J.R. Heath, S.C. O'Brien, R.F. Curl, R.E. Smalley, Nature 318 (1985) 62–163.
[16] X.M. Zhou, Z. Yang, H.G. Nie, Z. Yao, L.J. Zhang, S.M. Xiao, J. Power Sources 196 (2011) 9970–9974.
[17] J. Ahmed, Y. Yan, L.H. Zhou, S. Kim, J. Power Sources 208 (2012) 170–175.
[18] X. Wang, C.G. Hua, Y.F. Xiong, H. Liu, G.J. Du, X.S. He, J. Power Sources 196 (2011) 1904–1908.
[19] F. Bidault, A. Kucernak, J. Power Sources 196 (2011) 4950–4956.
[20] H. Dong, H.B. Yu, X. Wang, Q.X. Zhou, J.L. Feng, Water Res. 46 (2012) 5777–5787.
[21] C.C. Hu, S.C. Liao, K.H. Chang, Y.L. Yang, K.M. Lin, J. Power Sources 195 (2010) 7259–7263.
[22] H. Dong, H.B. Yu, X. Wang, Environ. Sci. Technol. 46 (2012) 13009–13051.
[23] M.S. El-Deab, T. Ohsaka, Angew. Chem. Int. Ed. 45 (2006) 5963–5966.
[24] Y.M. Tan, C.F. Xu, G.X. Chen, X.L. Fang, N.F. Zheng, Q.J. Xie, Adv. Mater. 22 (2012) 4584–4591.
[25] N. Omindea, N. Bartlett, X.Q. Yang, D.Y. Qu, J. Power Sources 195 (2010) 3984–3989.
[26] A. Verma, A.K. Jha, S. Basu, J. Power Sources 141 (2005) 30–34.
[27] F.Y. Cheng, Y. Su, J. Liang, Z.L. Tao, J. Chen, Chem. Mater. 22 (2010) 898–905.